THE ASTRONOMICAL JOURNAL, 116:489–498, 1998 July

DYNAMICS OF THE TRANS-NEPTUNE REGION: APSIDAL WAVES IN THE KUIPER BELT

WILLIAM R. WARD
Lunar and Planetary Institute,[1] 3600 Bay Area Boulevard, Houston, TX 77058; and Jet Propulsion Laboratory, California Institute of Technology, Pasadena, CA 91109

AND

JOSEPH M. HAHN
Lunar and Planetary Institute, 3600 Bay Area Boulevard, Houston, TX 77058
Received 1997 September 19; revised 1998 March 6

ABSTRACT

The role of apsidal density waves propagating in a primordial trans-Neptune disk (i.e., Kuiper belt) is investigated. It is shown that Neptune launches apsidal waves at its secular resonance near 40 AU that propagate radially outward, deeper into the particle disk. The wavelength of apsidal waves is considerably longer than waves that might be launched at Lindblad resonances, because the pattern speed, g_s, resulting from the apsis precesssion of Neptune is much slower than its mean motion, Ω_s. If the early Kuiper belt had a sufficient surface density, σ, the disk's wave response to Neptune's secular perturbation would have spread the disturbing torque radially over a collective scale $\lambda_* \approx r(2\mu_d \Omega/|\, r\, dg/dr\,|)^{1/2}$, where $\mu_d \equiv \pi\sigma r^2/(1\ M_\odot)$ and $\Omega(r)$ and $g(r)$ are respectively the mean motion and precession frequency of the disk particles. This results in considerably smaller eccentricities at resonance than had the disk particles been treated as noninteracting test particles. Consequently, particles are less apt to be excited into planet-crossing orbits, implying that the erosion timescales reported by earlier test-particle simulations of the Kuiper belt may be underestimated. It is also shown that the torque the disk exerts upon the planet (due to its gravitational attraction for the disk's spiral wave pattern) damps the planet's eccentricity and further inhibits the planet's ability to erode the disk.

Key words: celestial mechanics, stellar dynamics — comets: general — minor planets, asteroids

1. INTRODUCTION

In the past few years, the nature and dynamics of the Kuiper belt have been a subject of considerable attention. Interest was sparked by the demonstration by Duncan, Quinn, & Tremaine (1988) that a trans-Neptune disk could provide a plausible source for short-period comets. The discovery of the first Kuiper belt object, 1992 QB_1, by Jewitt & Luu (1992) further accelerated efforts of both observers and modelers. Great advances in both machine capability and computing techniques led to a series of increasingly intensive numerical experiments on the dynamics of test particles in the Kuiper belt region, e.g., Torbett (1989), Gladman & Duncan (1990), Holman & Wisdom (1993), Levison & Duncan (1993), and Duncan, Levison, & Budd (1995). These experiments made it clear that both secular and mean motion resonances play a major role in shaping the evolution of the Kuiper belt. Analytic treatments of Kuiper belt resonant dynamics have been provided by Morbidelli, Thomas, & Moons (1995) and Malhotra (1995, 1996).

To date, observations have yielded some 55 trans-Neptune bodies like 1992 QB_1. Based on the size of the sky area searched, estimates of the total population of such objects within 10° of the ecliptic and larger than 100 km are on the order of a few times 10^4. The total mass of the belt out to $\sim$50 AU from objects greater than $\sim$1 km in diameter is put at 0.06–0.25 Earth masses (M_E) (e.g., Jewitt, Luu, & Chen 1996; Stern 1996a).[2] However, these objects are far from uniform in their orbital characteristics. Most objects interior to $\sim$40 AU appear to reside in mean motion resonances with Neptune. These resonant orbits may be instrumental in preserving their occupants; it is well known that Pluto enjoys such protection through its 3:2 resonance with Neptune, which prevents close encounters between these objects. Resonant objects typically have high eccentricities, which may be evidence of resonance sweeping due to an outward migration of Neptune (Malhotra 1998).

The formation and possible migration of Neptune requires a few Neptune masses of material to be scattered by that planet (Fernández & Ip 1983, 1984, 1996), suggesting a primordial Kuiper belt considerably in excess of today's estimates if the belt extended smoothly into that region as well. Indeed, observations of extrasolar disks, such as β Pictoris, reveal remnant disks stretching far beyond the Sun-Neptune distance. In addition, the existence of 100 km–sized objects such as QB_1 has been interpreted as evidence of a much more massive (i.e., 10–50 M_E between 30 and 50 AU) primordial Kuiper belt. Stern and coworkers (Stern 1995, 1996a, 1996b; Stern & Colwell 1996) have pointed out that accretion in the *current* environment would not be possible, because of (1) high relative velocities, which are erosive, and (2) long collision timescales due to low number density. They argue that a much more massive and quiescent disk was needed in the past to account for the accretion of the largest objects so far observed. They postulate that this more massive disk may still exist beyond the gravitational influence of the giant planets, i.e., $r \gtrsim 50$ AU, and that the low-density region between there and Neptune may be highly depleted as a result of planetary perturbations. The current flux of short-period comets, which are suggested to originate from chaotic layers bounding low-order mean motion resonances (e.g., Malhotra 1996), may be the

[1] Visiting Scientist.

[2] The recent discovery of 1996 TL_{66} points to an additional scattered Kuiper belt component having a mass $\sim$0.5 M_E with orbits between $\sim$40 and 200 AU (Luu et al. 1997).

present-day manifestation of this erosion process. Numerical experiments show that many test particles achieve Neptune-crossing status within 1 Gyr (Levison & Duncan 1993; Duncan et al. 1995) due to the action of secular and mean motion resonances. These results are reminiscent of studies of the stability of test particles between the major planets (e.g., Franklin, Lecar, & Soper 1989; Duncan et al. 1988; Weibel, Kaula, & Newman 1990; Gladman & Duncan 1990; Soper, Franklin, & Lecar 1990; Holman & Wisdom 1993; Grazier et al. 1997).

It is very tempting to extend the numerical and analytic studies of test-particle behavior that have proved so valuable in explaining many of the emerging characteristics of the Kuiper belt to earlier epochs, when the belt was presumedly more massive. However, some caution is in order; test-particle integrations are strictly valid only when there are no interactions with other particles in the disk. And yet a motivation for postulating a much more massive primordial disk is to speed up accretion rates, i.e., to ensure more numerous collisions among the swarm. This may be a source of diffusion that is not included in the numerical models. Even more important are collective particle behaviors. These effects are long range and act continuously, not just during collisions. It is well known that a perturber orbiting in a fluid disk will launch density waves at resonances and that the resulting fluid motions are quite unlike that of an isolated particle subject to the same perturbations. The question is, when is a fluid model a more reasonable approximation of a particle disk than the motions of noninteracting members? In this paper, we explore that question for the particular case of a secular eccentricity resonance and show that the necessary conditions for wave action are easily satisfied. The resultant disk behavior is that of a one-armed spiral apsidal wave that propagates outward into the Kuiper belt. Apsidal waves have previously been reported in Saturn's rings (Cuzzi, Lissauer, & Shu 1981), where the apsidal precession rate of the ring particles is commensurate with the mean motion of the satellite Iapetus. However, this is the first application we are aware of in which the waves are launched from a true secular resonance, i.e., where the commensurability is between the apsidal rates of both perturber and disk particles. As we shall see, this has important implications for disk stirring and for the orbit of the perturber launching the waves.

In § 2, we review the behavior of an isolated particle that orbits near a secondary's secular resonance and calculate the particle's forced eccentricity as a function of semimajor axis. In § 3, these findings are contrasted with the motions that result when the disk has a nonnegligible self-gravity that allows for the propagation of density waves. Density wave theory is also used to compute the secondary's orbital evolution as it reacts to the waves it drives. Results are then summarized in § 4 with a discussion of how these findings may impact models of the primordial Kuiper belt.

2. TEST-PARTICLE MOTION

We begin by reviewing the behavior of a test particle orbiting near a secular resonance. Since particle orbits exterior to Neptune are to be examined, the weaker forcing terms due to the other planets are omitted. Neptune has a mass $M_s = 1.02 \times 10^{31}$ g, a semimajor axis $a_s = 30.1$ AU, orbital period $P_s = 165$ yr, eccentricity $e_s = 0.009$, and a precession rate of the longitude of perihelion $d\tilde{\omega}_s/dt \equiv g_s \approx g_8$, i.e., the frequency, $0\farcs673\ \mathrm{yr}^{-1}$ of the g_8 mode of the solar system, with corresponding period $P_{\tilde{\omega}} \sim 1.93 \times 10^6$ yr. This is the dominant term of the secular variation of Neptune's orbit (see, e.g., Applegate et al. 1986; Knežević et al. 1991). To first order in e_s, and fourth order in e, the particle's eccentricity, the secular perturbation potential due to the secondary is

$$\phi_s = -\mu_s a^2 \Omega^2 \left[\frac{1}{2} b_{1/2}^{(0)} + \frac{e^2}{8} \alpha b_{3/2}^{(1)} + \frac{e^4}{128} \alpha^3 \frac{d^2}{d\alpha^2} b_{3/2}^{(1)} - \frac{1}{4} e e_s \alpha b_{3/2}^{(2)} \cos(\tilde{\omega} - \tilde{\omega}_s) \right] \quad (1)$$

(e.g., Brouwer & Clemence 1961), where a and Ω are respectively the test particle's semimajor axis and mean motion, $\tilde{\omega}$ is its longitude of perihelion, $\mu_s \equiv M_s/(1\ M_\odot) = 5.15 \times 10^{-5}$, $\alpha \equiv a_s/a < 1$ in the Kuiper belt, and

$$b_{j/2}^{(m)}(\alpha) \equiv \frac{2}{\pi} \int_0^\pi \frac{\cos m\theta\, d\theta}{(1 - 2\alpha \cos\theta + \alpha^2)^{j/2}} \quad (2)$$

are Laplace coefficients. The secondary and particle orbits are assumed to be coplanar, and the elements subscripted s refer to the secondary.

Since the pattern speed, Ω_{ps}, is the precession rate, g_s, the Jacobi integral averaged over short-period terms is

$$J = E - \Omega_{ps} L = -(a\Omega)^2/2 + \phi_s - g_s a^2 \Omega \sqrt{1 - e^2}\ , \quad (3)$$

where E and L are the specific energy and angular momentum of the particle, respectively. To the same accuracy as equation (1), the normalized quantity $\hat{J} \equiv -2J/\mu_s(a\Omega)^2$, with $\varphi \equiv \tilde{\omega} - \tilde{\omega}_s$, can be written

$$\hat{J} = Ae^4 + Be^2 - Ce \cos\varphi + D\ , \quad (4)$$

$$A \equiv \frac{\alpha^3}{64} \frac{d^2 b_{3/2}^{(1)}}{d\alpha^2} - \frac{g_s}{4\mu_s \Omega}\ , \quad B \equiv \frac{\alpha}{4} b_{3/2}^{(1)} - \frac{g_s}{\mu_s \Omega}\ ,$$
$$C \equiv e_s \frac{\alpha}{2} b_{3/2}^{(2)}\ , \quad D \equiv b_{1/2}^{(0)} + \frac{2g_s}{\mu_s \Omega} + \frac{1}{\mu_s}\ . \quad (5)$$

A particle's semimajor axis does not vary as a result of secular forcing, so equation (4) may be used to construct phase-space plots along curves of constant $\hat{J}$ (level curves) to show how its eccentricity varies with the resonance angle φ. Figure 1*a* shows the level curves for $\hat{J} - D$ when $a = 1.37a_s$ ($\alpha \equiv a_s/a = 0.731$), while Figure 1*b* displays $\hat{J} - D$ versus e when $\sin(\tilde{\omega} - \tilde{\omega}_s) = 0$. The extrema, given by

$$\partial\hat{J}/\partial e = 4Ae^3 + 2Be \pm C = 0\ , \quad (6)$$

are the stationary points in Figure 1*a*. Phase-space trajectories tend to circle stationary points 1 and 2, while point C lies on the separatrix. Stationary-point positions are a function of the particle's semimajor axis. The site α where the particle's precession rate, $g(\alpha) = \frac{1}{4}\mu_s \Omega \alpha b_{3/2}^{(1)}(\alpha)$, matches the planet's precession rate, g_s, is identified as the resonance location in the lower order theory of Brouwer & Clemence; this site will be denoted here as α_0. The two branches of equation (6) can be computed numerically and are shown in Figure 2. However, simple analytic formulae are obtained by expanding equation (6) about α_0 where $B = 0$. The coefficient B can be replaced by $\sim B'\Delta a$, where $\Delta\alpha \equiv \alpha - \alpha_0$ and

$$B' \equiv \left.\frac{dB}{d\alpha}\right|_{\alpha_0} = \left.\frac{1}{4\alpha^{3/2}} \frac{d}{d\alpha} (\alpha^{5/2} b_{3/2}^{(1)})\right|_{\alpha_0}\ . \quad (7)$$

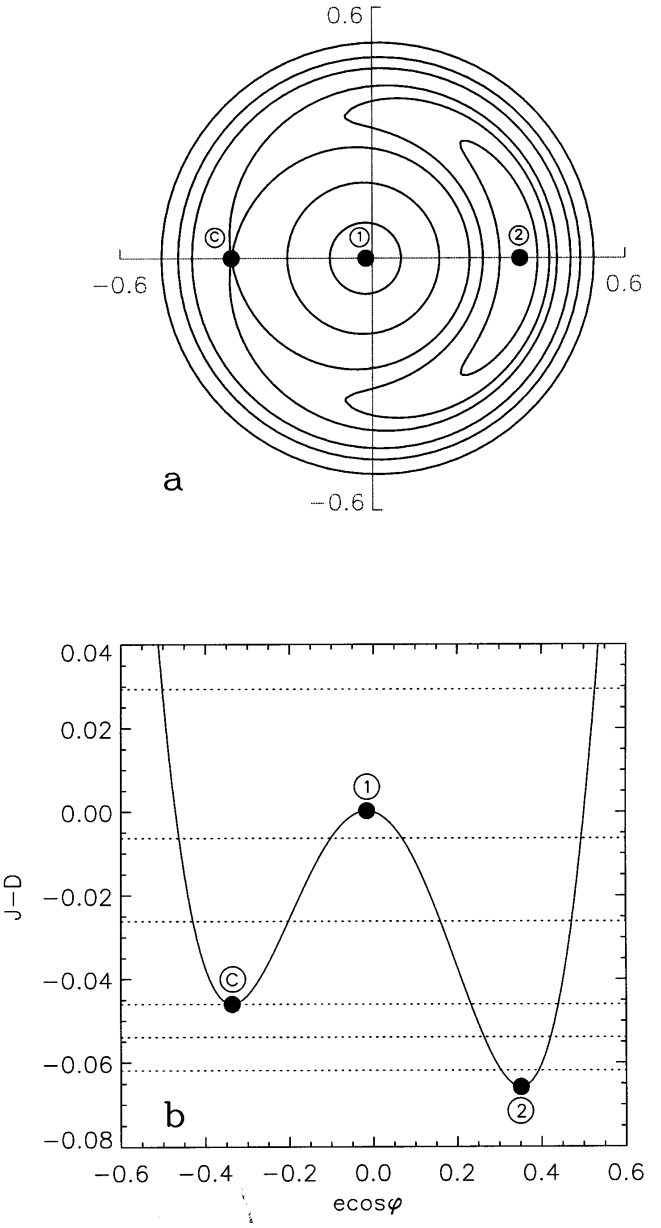

FIG. 1.—(*a*) $\hat{J}$ level curves for eq. (4). Each curve is a polar plot of eccentricity e vs. resonance angle φ for particles having the same semimajor axis, $\alpha = 0.731$, but different values of $\hat{J}$ (i.e., different free eccentricities). This and subsequent figures assume Neptune's mass and orbit. (*b*) The solid curve shows $\hat{J} - D$ vs. $e \cos \varphi$ (D is constant) when $\sin \varphi = 0$, and the dotted lines identify the values of $\hat{J} - D$ for each of the level curves in (*a*); the lowest dotted line refers to the smallest bean-shaped orbit in (*a*) while the upper dotted line is for the outermost orbit.

In this case, A and C can be evaluated at α_0 as well with little error. The reference value α_0 is now found from

$$\frac{1}{4}\alpha^{5/2} b_{3/2}^{(1)}\Big|_0 = \frac{g_s}{\mu_s \Omega_s} = 1.67 \,. \tag{8}$$

The left-hand side can be evaluated numerically from equation (2), which reveals that equation (8) is satisfied by the value $\alpha_0 = 0.770$. This implies that the resonance falls at $a_s/\alpha_0 = 39.1$ AU, which agrees reasonably well with the location of the g_8 resonance found by Knežević et al. (1991) when $I = 0$.

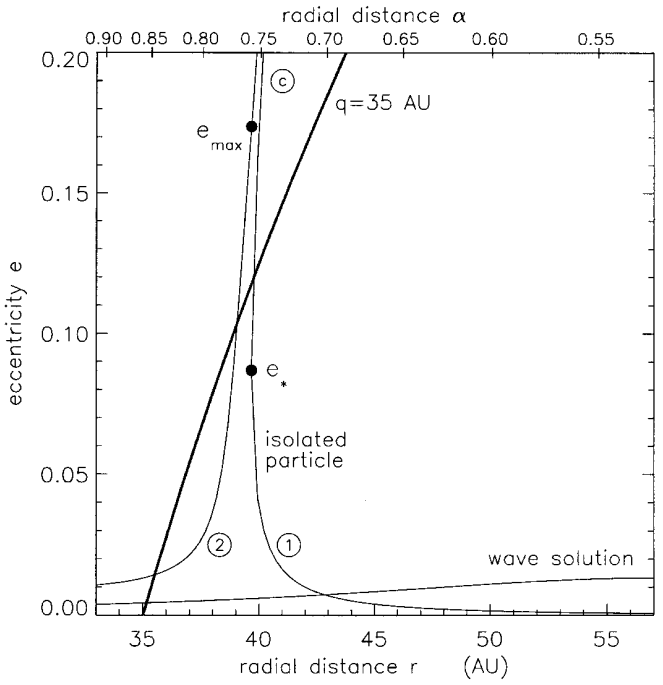

FIG. 2.—Particle's forced eccentricity e vs. semimajor axis (note that α increases to the left). The curve labeled "2" is the numerical solution to eq. (4) with $\cos \varphi = +1$, while the $\cos \varphi = -1$ solution has an upper (C) segment and a lower (1) segment. The lower portion of curve 2 left of $e_{\max}$ and the lower segment (1) represent the eccentricities that are likely adopted by a disk of initially cold particles. A filled circle indicates the maximum eccentricity $e_{\max} = 0.17$, which occurs a distance $\Delta\alpha_* \equiv -0.01$ from the resonance site α_0, consistent with the estimates given by eqs. (10) and (11). Also shown is the $e(\alpha)$ necessary for the perihelion distance, $q = 35$ AU, and the eccentricity from the wave solution for a $\mu_d = \mu_s$ disk.

The equilibrium e-values versus $\Delta\alpha$ are given by

$$\Delta\alpha = -2e^2 \frac{A}{B'} \mp \frac{1}{2e} \frac{C}{B'} \,. \tag{9}$$

The negative branch turns around (i.e., $de/d\,\Delta a = \infty$) at

$$e_* = \frac{1}{2}\left(\frac{C}{A}\right)^{1/3}, \quad \Delta\alpha_* = -\frac{3}{2}\frac{A}{B'}\left(\frac{C}{A}\right)^{2/3} . \tag{10}$$

At α_0, the ratios are $A/B' = 0.324$ and $C/A = 0.455 e_s$. Below e_*, the negative branch gives the eccentricity for point 1; above e_*, it is e of point C. The positive branch gives the eccentricity for point 2. This application considers a planet that has recently formed from a cool disk composed of noninteracting bodies,[3] so the particles' forced eccentricities will likely lie along the lower portions of the Figure 2 curves whenever they are multivalued. The resulting maximum e on the positive branch is $e_{\max} = 2e_* = (C/A)^{1/3}$. The corresponding e-values are

$$e_* = 0.385 e_s^{1/3} \,, \quad e_{\max} = 0.769 e_s^{1/3} \,. \tag{11}$$

For our adopted eccentricity ($e_s \simeq 0.01$), these become 0.083 and 0.166, respectively. But, as already mentioned, this treatment does not consider the additional perturbations that are also exerted by an ensemble of disk particles. How the disk's self-gravity affects the motions of its individual members is the subject of the remainder of this paper.

[3] For now, we assume that their free eccentricities due to gravitational relaxation of the disk can be neglected.

3. COLLECTIVE RESPONSE

3.1. *Scale Length*

Hahn, Ward, & Rettig (1995, hereafter HWR) have recently investigated a closely related problem: the effects of collective particle behavior on the trapping strength of mth-order Lindblad resonances for particles experiencing orbital decay due to gas drag. They found that the density wave response of the particle disk, of surface density σ, reduces the trapping strength by redistributing the angular momentum deposited at resonance over a collective scale length. When compared with particles treated in isolation, this phenomenon causes a strong reduction in the forced eccentricities. This length is roughly the distance, λ_*, that density waves can travel from resonance at their group velocity, $c_g \sim \pi G\sigma/\kappa$, during the libration time of the resonance variable. The libration frequency is $\dot{\varphi} = |\kappa - m|\Omega - \Omega_{\rm ps}||$, where $\Omega_{\rm ps}$ is the pattern speed and κ is the local epicyclic frequency of the disk. In terms of the so-called frequency distance from resonance, $D \equiv \kappa^2 - m^2(\Omega - \Omega_{\rm ps})^2 \approx 2\kappa(\kappa - m|\Omega - \Omega_{\rm ps}|)$, the libration frequency is $\dot{\varphi} \approx (\lambda/2\kappa)|dD/dr|$ with an average value equal to half the maximum. The libration time at distance λ_* becomes $\tau_{\rm lib} \approx 1/\langle\dot{\varphi}\rangle \approx 4\kappa/\lambda_*|dD/dr|$, where the derivative is evaluated at $D = 0$. Solving self-consistently, the scale length is of order[4]

$$\lambda_* \sim r\left|\frac{4\pi G\sigma}{r^2\, dD/dr}\right|^{1/2} \equiv r|2\epsilon|^{1/2}\,. \tag{12}$$

The collective behavior smooths out the perturbation, so that the torque cannot be *concentrated* on an annulus narrower than λ_*.

HWR argued that there are two necessary conditions for wave action: (1) there must be multiple particles present within the collective scale, and (2) their epicyclic radii must be less than the wavelength. We will tentatively assume that these conditions are met and check their validity a posteriori (§ 3.5). First, however, the amplitude of the disk's forced motions will be derived and compared with the isolated particle motions of § 2.

3.2. *Wave Solution for Secular Resonances*

A very readable account of the derivation of the first-order wave equation for a self-gravitating disk is given by Shu (1984). Following Shu, all perturbed quantities are assumed to be of the form $X \to Xe^{i(\omega t - m\theta)}$, where $\omega \equiv m\Omega_{\rm ps}$ is the forcing frequency, and the amplitude, ϕ', of the disk potential perturbation in the vicinity of resonance can be found from

$$r\frac{d\phi'}{dr} + \frac{irD\phi'}{2\pi G\sigma} = -\left(r\frac{d\phi_m}{dr} - \frac{2\phi_m}{\Omega_{\rm ps} - \Omega}\right) \equiv \psi\,, \tag{13}$$

which is obtained from Euler's and Poisson's equations (Shu 1984) and is valid in the tight-winding limit, $|d\phi'/dr| \gg |\phi'/r|$. For apsidal waves $m = 1$, and the forcing frequency $\omega = \Omega_{\rm ps} \equiv g_s$. The $m = 0$ potential can be combined with the central potential, $\phi_\odot$, and any *undisturbed* disk potential, ϕ_d, to determine the mean motion,

$$r\Omega^2 = \frac{d}{dr}(\phi_\odot + \phi_0 + \phi_d)\,. \tag{14}$$

From Goldreich & Tremaine (1980, their eq. [5]),[5] the secondary's potential is

$$\begin{aligned}\phi_s &= \sum_{l=-\infty}^{\infty}\sum_{m=0}^{\infty}\phi_{l,m}\cos\left[m\theta - m\Omega_s t - (l-m)\kappa_s t\right] \\ &= \sum_{l=-\infty}^{\infty}\sum_{m=0}^{\infty}\phi_{l,m}\cos\left[m\theta - (m-l)g_s t - l\Omega_s t\right]\,,\end{aligned} \tag{15}$$

where the relationship

$$g_s \equiv d\tilde{\omega}_s/dt = \Omega_s - \kappa_s \tag{16}$$

has been used. To get the secular terms, which do not contain $\Omega_s t$, set $l = 0$. For $e_s \ll 1$, the largest term in any amplitude is proportional to $e_s^{|l-m|} \to e_s^m$. For our purposes it is sufficient to retain only terms up to first order:

$$\phi_{\rm sec} \approx \phi_{0,0} + \phi_{0,1}\cos(\theta - g_s t)\,, \tag{17}$$

where, again from Goldreich & Tremaine (1980),

$$\begin{aligned}\phi_{0,0} &= -\frac{GM_s}{2a_s}\,b_{1/2}^{(0)}(\beta)\,, \\ \phi_{0,1} &= -e_s\frac{GM}{2a_s}\left[\beta\frac{d}{d\beta}\,b_{1/2}^{(1)} - b_{1/2}^{(1)}(\beta)\right],\end{aligned} \tag{18}$$

with $\beta \equiv r/a_s$, and the disk is assumed Keplerian.[6] (Henceforth the $l = 0$ part of the subscript will be dropped.)

The solution to equation (13) is

$$\phi' = \exp\left(-i\int\frac{D}{2\pi G\sigma}\,dr\right)\int_{r_e}^{r}\frac{\psi}{r}\exp\left(i\int\frac{D}{2\pi G\sigma}\,dr\right)dr\,, \tag{19}$$

where r_e denotes the inner boundary of the disk. For a secular resonance,

$$\begin{aligned}D &= \kappa^2 - (g_s - \Omega)^2 \approx 2\Omega(g_s - g)\,, \\ \left.\frac{dD}{dr}\right|_{r_0} &\approx -2\Omega\left.\frac{dg}{dr}\right|_{r_0}\,, \quad \epsilon = -\left.\frac{\mu_d\Omega}{r\,dg/dr}\right|_{r_0}\,,\end{aligned} \tag{20}$$

where $g(r) \equiv \Omega - \kappa$ is the apsis precession rate of the disk particles, with r_0 locating the secular resonance where $D(r_0) = 0$ and $g = g_s$, and where we have introduced the so-called normalized disk mass, $\mu_d \equiv \pi\sigma r^2/(1\ M_\odot) = \pi G\sigma/r\Omega^2$.

If $\lambda_* \ll |r_0 - r_e|$ and $g_s/|dg/dr|_{r_0}$, so that the collective scale is small compared with both the separation between resonance and disk edge and the scale over which a linear expansion, $D \approx (r - r_0)dD/dr|_{r_0}$, is reasonably good, equation (19) can be written in terms of Fresnel integrals:

$$\phi' = q(2\pi|\epsilon|)^{1/2}\psi_0\, H_q(\xi) \tag{21}$$

[4] Actually, eq. (12) underestimates the collective scale when λ_* becomes so long that dD/dr itself decreases significantly over that distance.

[5] Note that Shu's sign convention is the reverse of Goldreich & Tremaine's. We can bring eqs. (15) and (17) into compliance by multiplying the cosine arguments by -1.

[6] It is more convenient to develop the wave formalism in terms of β. Note, however, that this is the reciprocal of α used in § 2.

(see, e.g., Shu 1984), where

$$q = \mathrm{sgn}\left(\frac{dD}{dr}\right), \quad \xi \equiv q\,\frac{r - r_0}{r_0\sqrt{2\,|\,\epsilon\,|}}, \qquad H_q = \frac{1}{\sqrt{\pi}}\,e^{-iq\xi^2}\int_{-\infty}^{\xi} e^{iq\eta^2}\,d\eta\,, \tag{22}$$

and $\psi_0 \equiv \psi(\beta_0)$ is the value of the forcing function at resonance. If $g(r)$ decreases with heliocentric distance, then q is positive, and the direction of wave propagation is *outward*, i.e., deeper into the Kuiper disk. This is opposite to the propagation of waves launched from mean motion resonances in this region. The amplitude $|H_+(\xi)|$ vanishes as $\xi \to -\infty$ (non–wave side), but approaches unity as $\xi \to \infty$ (wave side). The streamlines of the motion are ellipses whose lines of apsides rotate in a clockwise manner with increased distance from resonance, thereby generating a one-arm spiral wave (e.g., Adams, Ruden, & Shu 1989).

To simplify ψ, note that $\phi_1 \propto \beta\, db_{1/2}^{(1)}/d\beta - b_{1/2}^{(1)}$ and make use of the fact that

$$\left(\beta\,\frac{d}{d\beta} + 2\right)\left(\beta\,\frac{db_{1/2}^{(1)}}{d\beta} - b_{1/2}^{(1)}\right) = \beta b_{3/2}^{(2)} \tag{23}$$

(Brouwer & Clemence 1961) to find

$$\psi = \tfrac{1}{2} e_s\,\beta b_{3/2}^{(2)}\,\mu_s\,a_s^2\,\Omega_s^2\,, \tag{24}$$

where the combination GM_s/a_s has been replaced by $\sim \mu_s a_s^2\,\Omega_s^2$. Substituting ψ into ϕ' yields

$$\phi' = \frac{e_s}{2}\,\mu_s\,\beta_0\,b_{3/2}^{(2)}(\beta_0)a_s^2\Omega_s^2\left(\frac{2\pi\mu_d\,\Omega}{|\,r\,dg/dr\,|}\right)_0^{1/2} H_+(\xi)\,, \tag{25}$$

where only ξ is allowed to vary, all other quantities being evaluated at resonance. Downstream, $|H_+| \to 1$, and Figure 3 shows $|\phi'|$ as a function of the disk's mass. Most of the driving occurs during the first wavelength, which increases with the square root of the disk mass, resulting in a similar increase in the amplitude.

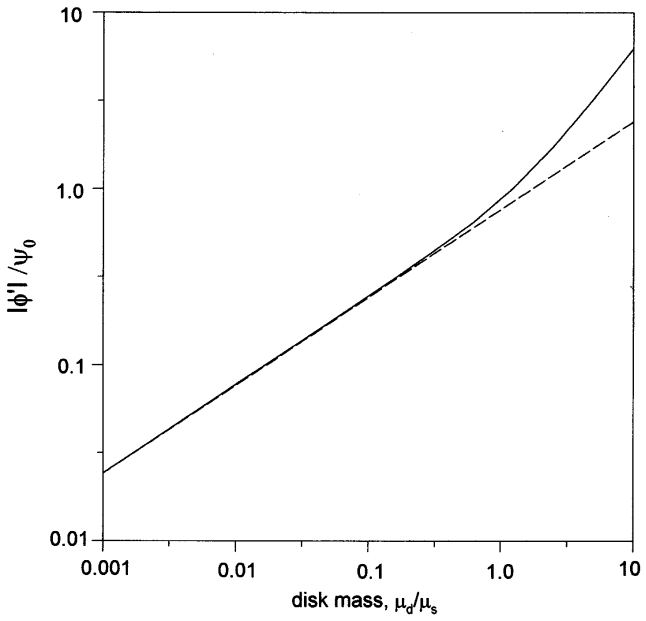

FIG. 3.—Absolute value of the downstream amplitude, $|\phi'|$, of the disk wave potential normalized to the resonance value of the forcing function, $\psi_0 \equiv \psi(\beta_0) = (e_s/2)\beta_0\,b_{3/2}^{(2)}(\beta_0)\mu_s(a_s\Omega_s)^2$. The dashed curve is the small-wavelength (low disk mass) solution (eq. [25]). The solid curve shows eq. (26) taking into account variations in the Laplace coefficients, which become more important as the wavelength increases.

At long wavelengths, setting all quantities except ξ to their values at resonance becomes more problematic. Equation (25) can be improved upon by including the most variable quantities, the Laplace coefficients, $b_{3/2}^{(m)}(\beta)$, inside the integrals. If $m(\beta - 1) \ll 1$, Laplace coefficients can be approximated by modified Bessel functions: $b_{3/2}^{(m)} \approx 2mK_1(m\,|\,\beta - 1\,|)/\pi\,|\,\beta - 1| \approx (2/\pi)(\beta - 1)^{-2}$. Using this, the wavenumber $rk \approx (2\pi)^{-1}(\mu_s/\mu_d)[(\beta_0 - 1)^{-2} - (\beta - 1)^{-2}]$, and the downstream value can be replaced by

$$|\,\phi'\,| = \pi(\beta_0 - 1)\psi_0\,|\,H_1^{(1)}(\Lambda)\,|\,, \tag{26}$$

where

$$\chi \equiv \frac{\beta - 1}{\beta_0 - 1}, \quad \Lambda \equiv \frac{2g_s(\beta_0 - 1)}{\mu_d\,\Omega_s}, \qquad H_1^{(1)}(\Lambda) = \frac{1}{\pi}\int_0^{\infty} \chi^{-2}e^{i\Lambda(\chi + \chi^{-1})/2}\,d\chi\,. \tag{27}$$

The last quantity above can be recognized as an integral representation of a Hankel function (see, e.g., Gradshteyn & Ryzhik 1965). Numerically, $\Lambda = 1.00(\mu_s/\mu_d)$, so that at low disk mass $\Lambda \gg 1$ and $H_1^{(1)}(\Lambda) \to (2/\pi\Lambda)^{1/2}\,\exp\,i(\Lambda - 3\pi/4)$. Substitution into equation (26) recovers equation (25), provided the identification $r\,dg/dr \equiv -2g/(\beta - 1)$ is made, which is consistent with our approximation of Laplace coefficients. However, for high-mass disks $\Lambda \ll 1$ and $H_1^{(1)}(\Lambda) \to 2i/\pi\Lambda$, and the wave potential increases linearly with disk mass. Equation (26) is also displayed in Figure 3. Strictly speaking, even equation (19) is an approximation, because its derivation ignores other slowly varying terms that may be significant at long wavelengths. Nevertheless, we see that equations (25) and (26) are useful approximations even up to $\mu_d \sim \mu_s$.

Wave driving is mostly limited to the distance over which the radial wavenumber, $k(r) \equiv D/2\pi G\sigma \approx (g_s - g)/\mu_d\,r\Omega$, increases rapidly with r. The concomitant shortening of the wavelength is necessary for a net angular momentum flux to develop. Figure 4 displays wavenumber, k, versus r for three values of the disk mass,[7] $\mu_d(r_s) \equiv \mu_{d,s}$, for a power-law disk, $\sigma \propto r^{-n}$, with $n = 2$ including variation of all quantities. In each case, the most rapid increase in wavenumber occurs within the first $\delta r \approx O(10)$ AU. The wavelength, $\lambda(r)$—as defined by $\Phi(r + \lambda) - \Phi(r) = 2\pi$, where the phase $\Phi(r) \equiv \int k\,dr$—is shown in Figure 5 for the same disk masses as in Figure 4. The curves start at 39.1 AU with the value of the first wavelength.

3.3. *Resonance Site*

The amplitude of the disk's wave response is sensitive to the location of the resonance, which itself can depend upon the disk's potential (e.g., Ward 1981). To determine the resonance site self-consistently, write the precession rate of a test particle's longitude of perihelion as

$$g = \frac{d\tilde{\omega}}{dt} \approx \frac{-1}{ea^2\Omega}\,\frac{\partial\phi_T}{\partial e}\,, \tag{28}$$

where $\phi_T \equiv \phi_\odot + \phi_s + \phi_d + \phi'$ is the sum of all the contributing potentials. The central $\phi_\odot \propto 1/r$ potential can be ignored because it cannot produce precession. Using the

[7] As defined, $\mu_d \equiv \pi\sigma r^2/(1\,M_\odot)$ varies as r^{2-n}.

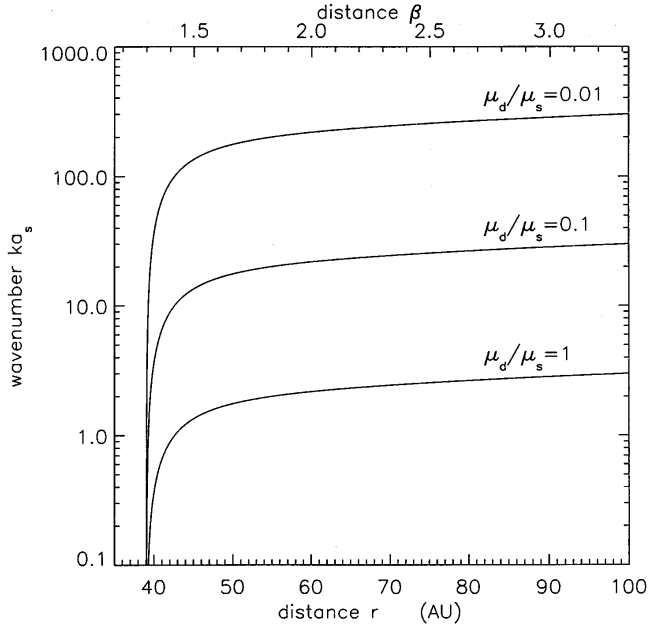

FIG. 4.—Wavenumber as given by the dispersion relationship, $k = D/2\pi G\sigma \sim (g_s - g)/\mu_d(r\Omega)$, which increases rapidly as $g(r)$ drops, and then more slowly as $r^{n-3/2}$, for a $\sigma \propto r^{-n}$ disk. The case shown is for $n = 2$. Curves are parameterized by the disk-to-secondary mass ratio with μ_d evaluated at a_s.

disturbing function (eq. [1]) to order e^2, ee_s, yields the familiar expression

$$\left.\frac{d\tilde{\omega}}{dt}\right|_s \approx \mu_s \Omega\left[\frac{1}{4}\,\alpha b_{3/2}^{(1)} - \frac{1}{4}\,\frac{e_s}{e}\,\alpha b_{3/2}^{(2)}\cos(\tilde{\omega} - \tilde{\omega}_s)\right] \quad (29)$$

for the precession rate of an isolated test particle. The nominal resonance position, α_0, is where the first term equals the precession rate of the secondary, g_s, while the second term is used to "tune" the rate to the resonance value for particles inside and outside of resonance. As the resonance is approached, the eccentricity (in this linear treatment) must diverge to shut off the second term when it is not needed. In § 2, this singularity was removed by including e^4 terms in the disturbing function. However, disk gravity will also remove the divergence, as discussed below.

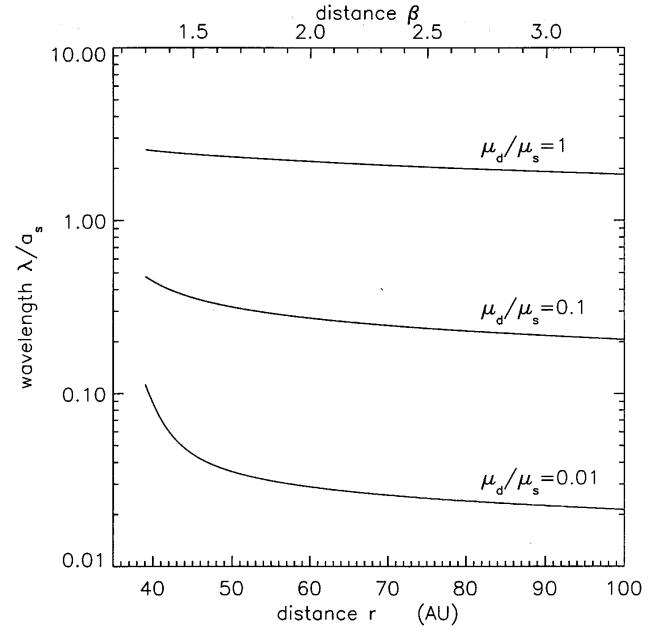

FIG. 5.—Wavelength, $\lambda(r)$, defined by the relationship $\int_r^{r+\lambda(r)} k\,dr = 2\pi$, for the same cases as shown in Fig. 4. The beginning of each curve marks the value of the first wavelength. For higher mass disks, the first wavelength extends beyond the rapid rise in k so that a precipitous drop in wavelength is not observed.

Ward (1981; see also Heppenheimer 1980) showed that an axisymmetric disk of surface density $\sigma \propto r^{-n}$ produces an additional potential,

$$\phi_d = -2\pi G\sigma r \sum_{j=0}^{\infty} \frac{(4j+1)[(2j)!/2^{2j}(j!)^2]^2}{(2j+2-n)(2j-1+n)} = -2\pi G\sigma r c_n\,, \quad (30)$$

which also affects the precession rate. An easy way to show this is by writing $\kappa^2 = r\,d\Omega^2/dr + 4\Omega^2$ so that $\kappa^2 - \Omega^2 = r\,d\Omega^2/dr + 3\Omega^2 = r^{-2}\,d(r^3\Omega^2)/dr$. Approximating $\kappa^2 - \Omega^2 = (\kappa + \Omega)(\kappa - \Omega) \approx -2\Omega\,d\tilde{\omega}/dt$ and using equation (14) allows one to find the precession rate. The addition contribution from the undisturbed disk is

$$\left.\frac{d\tilde{\omega}}{dt}\right|_d = \frac{-1}{2r^2\Omega}\frac{d}{dr}\left(r^2\frac{d\phi_d}{dr}\right) = -C_n\mu_d\Omega\,, \quad (31)$$

which must be added to the right-hand side of equation (29), where $C_n \equiv (n-1)(2-n)c_n$. For a fair range of n, $C_n \approx O(1)$, and equation (31) describes apsidal line *regression*, which shifts the resonance location inward toward the secondary (Ward 1981; see also Levison, Stern, & Duncan 1998).

Remembering that wave behavior of the disk results in a much reduced eccentricity compared with the isolated particle case, the second term in equation (29) can no longer vanish as a result of a divergence of e. On the other hand, there is an additional part of the potential due to the spiral wave, ϕ', yet to consider. It is shown in Appendix A that these two nonaxisymmetric terms cancel, leaving

$$\frac{1}{4}\,\alpha^{5/2}b_{3/2}^{(1)} - C_n\left(\frac{\mu_{d,s}}{\mu_s}\right)\alpha^{n-1/2} = \frac{g_s}{\mu_s\Omega_s} \quad (32)$$

as the resonance condition. The disk correction to the resonance location is small for disks of moderate mass, i.e., $\mu_{d,s} \lesssim \mu_s$. In this case, the resonance condition is approximately that used in § 2. The gradient of the precession frequency is then

$$r\frac{dg}{dr} \approx -\frac{1}{4}\,\mu_s\Omega_s\,\alpha\frac{d}{d\alpha}\,[\alpha^{5/2}b_{3/2}^{(1)}(\alpha)] \equiv -\Gamma(\alpha)g_s\,, \quad (33)$$

where $\Gamma(\alpha)$ is a function of semimajor axis but does not depend explicitly on Laplace coefficients (Appendix B). For $\alpha = 0.770$, $\Gamma = 9.11$.

3.4. *Eccentricities*

Using the formulae developed above, we arrive at the forced eccentricities of a self-gravitating disk. In the tight-winding limit, the fluid disk's radial velocity is $U \approx \phi'\Omega/2\pi G\sigma$ (e.g., HWR), while the eccentricity is

$$e_{\rm dw} = \left|\frac{U}{r\Omega}\right| \approx \frac{1}{4}\,e_s\mu_s\,\alpha b_{3/2}^{(2)}(\alpha)\left(\frac{2\pi}{\mu_d}\right)^{1/2}\left(\frac{Q}{|r\,dg/dr|}\right)^{1/2}|H_+|\,, \quad (34)$$

with all but $|H_+|$ being evaluated at resonance. In equation (34) the Laplace coefficient is written in terms of $\alpha \equiv 1/\beta$, by making use of the identity $b_{j/2}^{(m)}(\beta) = \alpha^j b_{j/2}^{(m)}(\alpha)$. Substituting equations (8) and (33) and evaluating $b_{3/2}^{(2)}(\alpha_0) = 11.19$ yields

$$e_{\rm dw} \approx 1.1 e_s (\mu_s/\mu_d)^{1/2} |H_+| \,. \tag{35}$$

Equation (34) is compared with test-particle behavior in Figure 2 for the case $\mu_d = \mu_s$. The collective response of the disk suppresses the particles' eccentricity below the isolated particle value, $e_{\rm max} \sim 0.769 e_s^{1/3}$, when $\mu_d/\mu_s \gtrsim 2.4 e_s^{4/3}$, which for $e_s \sim 0.01$ reads 5×10^{-3}. Hence, for low-mass disks with $\mu_d \lesssim 10^{-2}\mu_s$, collective behavior is not important. However, for higher mass the forced eccentricity is reduced by the wave action. For a disk mass comparable to Neptune, the full amplitude eccentricity is $e_{\rm dw} \sim 0.011$, which is down by a factor of $e_{\rm dw}/e_{\rm max} \sim 1.4 e_s^{2/3} = 0.065 \approx 1/15$. At the resonance itself, $|H_+| = \frac{1}{2}$, and the eccentricity is only half its downstream value.

3.5. *Wave Criteria*

As advertised, we now return to the issue of whether the necessary conditions for wave action are met. Without collective behavior, the orbit crossing half-width[8] of the resonance for a noninteracting, isolated particle can be estimated as $w \sim (\psi/r\, dD/dr)^{1/2}$. The wave response will be linear with nested orbits if $\lambda_* > w$, i.e., when $\psi \lesssim 4\pi G\sigma r$. From equation (24), $\psi \sim O(e_s \mu_s r^2 \Omega^2)$, and the linearity criterion reads $4\mu_d \gtrsim e_s \mu_s \sim 10^{-2}\mu_s$.

Another concern is whether the presence of other resonances, e.g., the 2:1 mean motion resonance, could interfere with wave action at the secular resonance. The behavior of mean motion resonances when modified by the Kuiper belt's self-gravitation is yet to be examined, but we speculate that if their orbit-crossing half-width [$\psi_m \sim O(m\mu_s a_s^2 \Omega_s^2)$, $r\, dD/dr \approx 3m\Omega_s\Omega$, and $w \sim O(r\mu_s^{1/2})$] is significantly less than the apsidal wavelength, the effects on apsidal wave generation will be minor. This requires $\mu_d/\mu_s \gg g_s/\Omega_s \sim O(10^{-4})$, which is easily satisfied.

Next, we check to see when the epicyclic radius, $\sim v_{\rm disp}/\Omega$, due to any dispersion velocity, $v_{\rm disp}$, among the particles becomes comparable to the wavelength. Disk stability requires a minimum dispersion velocity of $v_c = 1.07\pi G\sigma/\kappa \approx \mu_d r\Omega$ regardless of particle size (Toomre 1964). If the typical particles are large enough that their escape velocities exceed this, they will have dispersion velocities $v_{\rm disp} \sim v_{\rm esc}$. Call $v_{\rm disp}/v_c \equiv Q$, so that $v_{\rm disp} \simeq \mu_d Q(r\Omega)$; the reader will recognize Q as the well-known Toomre stability parameter. Setting $v_{\rm disp}/\Omega \sim |k|^{-1}$, and assuming downstream behavior for k where g can be ignored, the location β_Q of the wave propagation barrier is given by

$$\beta_Q^n \sim (\Omega_s/g_s) Q_s^{-1} \,, \tag{36}$$

where $Q_s \equiv Q(r_s)$ is to be evaluated for an unperturbed disk at the distance of the secondary's orbit.

Kuiper disk objects with escape velocities comparable to stability minimum have radii $R_c = \mu_d (r\Omega)(8\pi G\rho/3)^{-1/2} \sim 0.2(\mu_d/\mu_s)$ km for $\rho \sim 2$ g cm^{-3}. Therefore, $Q_s = R/R_c \sim 5(\mu_s/\mu_{d,s})[R/(1\ \text{km})]$ for $R > R_c$, and $\beta_Q^n = 2.3 \times 10^3 (\mu_{d,s}/\mu_s)[R/(1\ \text{km})]^{-1}$, i.e., $\sim$450 AU in an $n = 2$ Neptune-mass disk composed of 10 km Kuiper objects, 140 AU if most of the mass is in 100 km objects. For $n = 3/2$, these distances increase to $\sim$1100 and $\sim$240 AU, respectively. (A better estimate of the distance to the Q-barrier can be found by including the Toomre reduction factor in the dispersion relation; see Toomre 1964; HWR; Hahn & Ward 1998.)

Next check the requirement that there be multiple particles within a wavelength. Downstream, where k changes little during a given cycle, we can write

$$\lambda = \frac{2\pi}{k} \to 2\pi r \frac{\mu_d \Omega}{g_s} \approx 3.8 a_s \beta^{3/2-n} \frac{\mu_{d,s}}{\mu_s} \,. \tag{37}$$

Because waves from a secular resonance can be extremely long, $\lambda \sim O(10^2 \mu_d/\mu_s)$ AU, this requirement is easily satisfied, i.e., the typical spacing between particles is $\sim N^{-1/2}$, where $N \equiv \sigma/M$ is the surface number density of objects of mass M. $\rm QB_1$ objects have masses of order $10^{-6}\ M_{\rm E}$; for this mass, $\lambda N^{1/2} \sim O(10^4)(\mu_d/\mu_s)^{3/2}$. If the bulk of the material is in smaller objects, $R < 100$ km, there is an additional factor of $(10^2\ \text{km}/R)^{3/2}$.

3.6. *Secondary's Orbit*

The reaction torque, $T_s = -T = r\phi'^2/4G$, on the secondary can have important effects on its orbit (see, e.g., Goldreich & Tremaine 1980). The secondary's angular momentum and energy are $L = M_s a_s^2 \Omega_s (1 - e_s^2)^{1/2}$ and $E = -M_s (a_s \Omega_s)^2/2$. Differentiating with respect to time and rearranging yields $\dot{a}_s/a_s = -\dot{E}/E$ and $\dot{e}_s/e_s = -e_s^{-1}(1 - e_s^2)^{1/2}(\dot{L}/L + \dot{E}/2E)$, where $\dot{L} = T_s$. Since a wave potential appears stationary in a reference frame rotating at its pattern speed, the rates of change are related by $\dot{E} = \Omega_{\rm ps}\dot{L}$, by virtue of the Jacobi constant. From this, semimajor axis and eccentricity variation rates can be derived:

$$\frac{\dot{a}_s}{a_s} = \frac{2T_s}{M_s a_s^2 \Omega_s} \frac{\Omega_{\rm ps}}{\Omega_s} \,, \quad \frac{\dot{e}_s}{e_s} = \frac{-T_s}{M_s e_s^2 a_s^2 \Omega_s} \left(1 - \frac{\Omega_{\rm ps}}{\Omega_s}\sqrt{1 - e_s^2}\right). \tag{38}$$

Substituting the torque and pattern speed, g_s, for the secular resonance in the equation for e_s yields

$$\left.\frac{1}{e_s}\frac{de_s}{dt}\right|_{\rm sec} \sim -\frac{\pi}{4}\beta^{3/2}[b_{3/2}^{(2)}(\beta)]^2 \mu_d \mu_s \Omega_s \left(\frac{\Omega_s}{-r\, dg/dr}\right)$$

$$\sim -1.66 \mu_d \mu_s \Omega_s \frac{\Omega_s}{g_s} \,, \tag{39}$$

and the eccentricity decays. From equation (38), it follows that the ratio $|\dot{e}_s/e_s|/|\dot{a}_s/a_s| = [\Omega_s/\Omega_{\rm ps} - (1 - e_s^2)^{1/2}]/2e_s^2 \approx \Omega_s/2e_s^2 g_s \gg 1$, so that the semimajor axis changes little during the decay of the eccentricity.

Equation (39) should be compared with the excitation rate from Lindblad resonances,

$$\left.\frac{1}{e_s}\frac{de_s}{dt}\right|_{\rm L} \sim \frac{m_{\rm max}^4}{12\pi} \mu_d \mu_s \Omega_s \left[\frac{19}{4} K_1\left(\frac{4}{3}\right) + 5K_0\left(\frac{4}{3}\right)\right]^2$$

$$\sim 0.048 \mu_d \mu_s \Omega_s \left(\frac{a_s}{\Delta r}\right)^4 \tag{40}$$

[8] This is the distance inside which orbits intersect. It is different than the *amplitude* half-width, which varies as $\psi^{2/3}$.

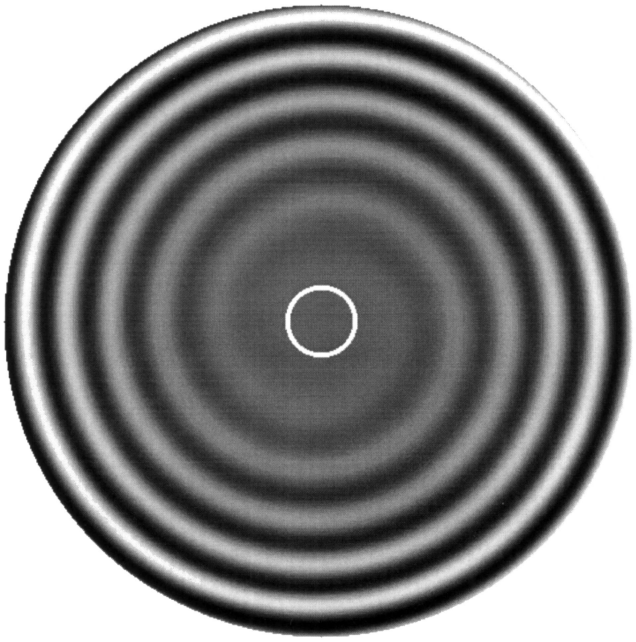

FIG. 6.—Surface density perturbation in an $n = 2$ disk for an one-armed trailing apsidal wave generated in an extended Kuiper belt by a secondary at 30.1 AU with normalized disk and secondary masses comparable to Neptune's mass. The white circle indicates the resonance site at 39.1 AU. Crests of the waves are white; the grayscale is stretched to reveal the contrast. The surface density amplitude can be found from eq. (43). The first wavelength is ~ 75 AU, in agreement with the $\mu_d/\mu_s = 1$ curve of Fig. 5, and decreases as $r^{-1/2}$. These waves are predicted to become nonlinear at ~ 330 AU, which is near the edge of the plot.

(Goldreich & Tremaine 1980; Ward 1988), where $m_{\max}$ is the highest order Lindblad resonance falling in a disk with an inner edge a distance $\Delta r = r_e - a_s$ from the secondary. Unlike $(\dot{e}_s/e_s)_{\rm sec}$, equation (40) falls off rapidly as Δr is increased. Thus, Lindblad resonances cannot prevent the decay of the eccentricity if the distance to the inner edge exceeds $\Delta r \sim 0.4 a_s (g_s/\Omega_s)^{1/4} \approx 0.04 a_s \sim 1.2$ AU, which is comparable to the edge of the chaotic zone. When the secular resonance dominates, e_s decays with a characteristic timescale of $\tau_{\rm decay} \sim 5.2 \times 10^5 \mu_s/\mu_d$ yr, and the disk torque on the secondary quickly damps its orbital eccentricity.[9]

4. DISCUSSION

Figure 6 plots the perturbed surface density for $\mu_d/\mu_s = 1$, found from the WKB solution to Poisson's equation for ϕ':

$$\sigma' = \frac{i}{2\pi G r^{1/2}} \frac{d}{dr} (r^{1/2} \phi') \tag{41}$$

(e.g., Goldreich & Tremaine 1978, 1980). The long wavelength keeps the response linear at launch because nonlinear forcing only occurs when $e_{\rm dw} \gtrsim \lambda_*/r$ (see, e.g., HWR), for which $\mu_d/\mu_s \lesssim O(10^{-2})$. For larger disks, the forcing at resonance is linear.

Nonlinearity *can* develop downstream if the waves wind up and/or the surface density drops sufficiently. The fractional perturbation of the wave, σ'/σ, is found from the conservation of angular momentum luminosity

$$|\mathscr{L}| = m\pi^2 G r \left|\frac{\sigma'}{k}\right|^2 = \frac{m r \phi'^2}{4G} \approx \left.\frac{m\pi^2 \sigma \psi^2}{|r\, dD/dr|}\right|_0 \tag{42}$$

(Toomre 1964; Goldreich & Tremaine 1978), where the right-hand side is to be evaluated at resonance. For our Neptune model, the fractional density perturbation is

$$\frac{\sigma'}{\sigma} = e_s \alpha_0^{(2n+5)/4} b_{3/2}^{(2)} \left(\frac{\mu_s}{\mu_{d,s}}\right)^{3/2} \left(\frac{g_s}{\mu_s \Omega_s}\right)^{1/2} \left(\frac{\pi}{8\Gamma}\right)^{1/2} \left(\frac{r}{a_s}\right)^{2(n-1)}$$
$$\approx 1.1 e_s \left(\frac{\mu_s}{\mu_{d,s}}\right)^{3/2} \alpha_0^{n/2} \left(\frac{r}{a_s}\right)^{2(n-1)} . \tag{43}$$

For $n = 2$, σ'/σ approaches unity at $r \approx 1.1 e_s^{-1/2} (\mu_{d,s}/\mu_s)^{3/4} a_s$, which for $e_s = 0.01$, $a_s \sim 30.1$ AU, and $\mu_{d,s} \sim \mu_s$ reads $r \sim 330$ AU. Nonlinear waves may shock-dissipate, depositing their energy and angular momentum in remote regions of the disk. The large wavelengths of apsidal waves may also render them detectable in extrasolar disks. This issue is to be addressed in a follow-up paper (Hahn & Ward 1998).

Long-term test-particle integrations have shown that Neptune will eject bodies with $q < 35$ AU over timescales of less than 10^9 yr (Duncan et al. 1995). The removal of test particles with $a < 35$ AU is likely assisted by Neptune's mean motion resonances. However, it appears that the mean motion resonances must play a lesser role in stirring and depleting the more distant parts of a Kuiper belt composed of test particles. The Jacobi constant for a particle at an $(m + 1):m$ mean motion resonance has the same form as equation (4) but with $A \approx 3(m + 1)^2/4$ and $C \approx 8m\mu_s/5$ (e.g., Peale 1986), so the particle's maximum eccentricity is

$$e_{\max} = (C/A)^{1/3} \approx (2.1\mu_s/m)^{1/3} (1 + 1/m)^{-2/3}$$
$$\approx 0.05 m^{-1/3} (1 + 1/m)^{-2/3} ,$$

and its perihelion is $q = a_s[(1 + 1/m)^{2/3} - 0.05/m^{1/3}] > 35$ AU for all of the $m \leq 3$ resonances that lie beyond 35 AU. Therefore, it appears that the g_8 resonance is the most significant in-plane perturbation exerted by Neptune in the more distant parts of the Kuiper belt. In § 2, it was confirmed that the perturbations exerted on a massless test particle at the g_8 resonance are sufficiently vigorous to excite its eccentricity and lower its perihelion below 35 AU for a range of semimajor axes. Consequently, this resonance may act as a particle sink in the *current* Kuiper belt, since nearby particles may diffuse into the resonance.

Although long-term test-particle integrations shed light on the later behavior of the Kuiper belt, they appear less credible for its earliest stage, when its mass may have been much larger. The self-gravity of the disk cannot be ignored, and the particles can respond in a collective (i.e., wave) mode. At a secular resonance, the necessary conditions for wave action are easily satisfied, and Neptune launches apsidal waves that propagate outward into the Kuiper belt. The wave response spreads Neptune's torque over the collective scale, resulting in significantly *lower* particle eccentricites than predicted by the isolated particle treatment. The particle motions are coherent and nested and do not contribute to a dispersion velocity. Since test-particle simulations do not consider particle-particle interactions, they fail to account for this transport of density waves, and thus,

[9] Actually, the torque from an *interior* secular resonance would excite the eccentricity (Hahn & Ward 1998), but here we assume that the interior planetesimal disk has been swept up by planet formation by the time Neptune forms.

the reliability of their findings is uncertain. For a secular resonance at ~ 39 AU in a $\mu_d \approx \mu_{\rm Nep}$ disk, particles acquire insufficient eccentricities to have their perihelia within 35 AU of Neptune. Indeed, it seems problematic whether this secular resonance could contribute significantly to the depletion of the Kuiper belt in an early, high-mass stage, unless it somehow acts in concert with other resonances in an as yet unknown manner. This caveat may also apply to other situations treated by test-particle integrations, such as the depletion of the asteroid belt and of planetesimals between the planets.

The lowest mass estimate of the primordial Kuiper belt obtained via a test-particle simulation is given in Figure 8 of Duncan et al. (1995), who require an initial number density profile of $n(r) \sim 3 \times 10^6 (40\ {\rm AU}/r)^2$ particles ${\rm AU}^{-2}$ to account for the present flux of Jupiter-family comets into the inner solar system. This implies an initial surface density of $\sigma \sim 0.06[R/(10\ {\rm km})]^3$ g cm^{-2} or $\mu_d/\mu_s \sim 0.7[R/(10\ {\rm km})]^3$ at 40 AU, assuming a mass density of 1 g cm^{-3}. Since the bulk of these objects must be comet-sized, R is likely $\sim$1–10 km. Inserting this disk mass into the discussion of § 3.5 shows that, even at the low end, the criteria for apsidal wave propagation are marginally met, although the waves may be nonlinear. Again, these models do not allow for the defocusing of the planet's disturbance at resonance due to the disk's self-gravity, and, as a result, the erosion rates reported in Duncan et al. (1995) may be overestimated.

A substantial disk is required by models in which the giant planets migrate (e.g., Fernández & Ip 1983, 1984, 1996; Malhotra 1995, 1996). For instance, Malhotra (1998) estimates that $\sim 35\ M_{\rm E}$ of disk material distributed between the giant planets is necessary to expand Neptune's orbit such that Pluto is captured at a mean motion resonance with its eccentricity pumped up to the observed value. If one spreads this amount of disk material between the giant planets as per an r^{-2} surface density distribution and then extrapolates additional mass beyond Neptune's orbit,[10] then the inferred disk mass is $\mu_d/\mu_s \sim 0.6$.

A similarly massive primordial Kuiper belt has been postulated by Stern (1996a, 1996b), who prefers $\sim$10–50 $M_{\rm E}$ of material between 30 and 50 AU (i.e., $\mu_d/\mu_s \sim 0.6$–3 for an r^{-2} surface density distribution) in order to collisionally assemble $\sim$100 km–sized QB_1-type Kuiper belt objects prior Neptune's formation. In this scenario, Neptune forms after $\sim 10^8$–10^9 yr and is then presumed to stir up the disk so much that further growth of QB_1 objects is halted. Although Neptune's shorter wavelength Lindblad waves will be shut off once the particles achieve that size, Neptune's apsidal waves still propagate. If this scenario is to succeed, then it remains to be demonstrated whether Neptune can actually stir up this massive disk in order to shut off its apsidal waves, truncate particle growth at QB_1 sizes, and also deplete the disk to its current low-mass state.

Neptune's ability to erode a massive primordial disk is further inhibited by the torque that the disk exerts upon the planet. The torque between planet and disk is surprisingly strong, because the long wavelengths allow the disk to couple to the forcing potential over large distances. As a result, Neptune's eccentricity-damping timescale could be quite short as compared with the age of the solar system, which obviously contradicts Neptune's finite (though curiously low) eccentricity. One possible resolution to this dilemma is that an extended, high-mass Kuiper belt beyond 50 AU does *not* exist and the drop-off in surface density past Neptune is a remnant of the true edge of the primordial planetesimal disk. Alternatively, sufficient erosion of the disk beyond the secular resonance could shut down the wave response. However, we have seen that collective behavior may inhibit erosion, so a better treatment of this problem, including Lindblad resonances, is needed. Still another possibility is that waves reflect off the Q-barrier or a real disk edge before damping and return their energy and angular momentum to the resonance zone. At any rate, the requirement that Neptune's present eccentricity—or, more precisely, the amplitude of the g_8 mode—be finite could be used to place a rather stringent constraint on the mass and distribution of the current Kuiper belt. This important topic is addressed in another paper, viz., Ward & Hahn (1998).

This paper represents contribution 944 from the Lunar and Planetary Institute, which is operated by the Universities Space Research Association under NASA contract NAGW-4575. W. R. W. thanks the Lunar and Planetary Institute for their hospitality during a portion of this effort. We acknowledge informative discussions with Hal Levison and Alan Stern at the Southwest Research Institute and careful reviews of the manuscript by Renu Malhotra and S. Stepinsky at LPI. A portion of this research was also carried out at the Jet Propulsion Laboratory, California Institute of Technology, under contract with the National Aeronautics and Space Administration.

[10] Although it should be said that extending the disk well beyond Neptune is an additional assumption not required by the migration hypothesis.

APPENDIX A

To calculate the effect of the wave potential on a particle's precession rate, Gauss's form of Lagrange's equation is employed:

$$\frac{d\tilde{\omega}}{dt} = \frac{\sqrt{1-e^2}}{ea\Omega}\left[-F_r \cos f + F_\theta\left(\frac{r}{p}+1\right)\sin f\right], \tag{44}$$

where f is the true anomaly, F_r and F_θ are radial and azimuthal perturbation forces, respectively, and $p \equiv a(1-e^2)$. In the tight-winding limit, $|\partial\phi'/\partial r| \gg (1/r)|\partial\phi'/\partial\theta|$, which implies $|F_r| \gg |F_\theta|$, so we drop the second term and set

$$F_r \approx {\rm Re}\,[e^{-i(f+\tilde{\omega}-\tilde{\omega}_s)}(-d\phi'/dr)]\ . \tag{45}$$

The wave potential satisfies equation (13). For a test particle at resonance $D = 0$, and the orbit-averaged contribution of the

wave potential to the precession rate becomes

$$\left.\frac{d\tilde{\omega}}{dt}\right|_w = \frac{\psi}{2ea^2\Omega}\cos(\tilde{\omega} - \tilde{\omega}_s)\,. \tag{46}$$

Substituting for ψ reveals that equation (46) cancels the problematic e_s/e term in equation (29).

APPENDIX B

The derivative of g is

$$r\frac{dg}{dr} = -\frac{1}{4}\mu_s\Omega_s\alpha^{5/2}\left(\frac{5}{2} + \alpha\frac{d}{d\alpha}b^{(1)}_{3/2}\right). \tag{47}$$

From Brouwer & Clemence (1961),

$$\alpha\frac{d}{d\alpha}b^{(1)}_{3/2} = \frac{1+4\alpha^2}{1-\alpha^2}b^{(1)}_{3/2} - \frac{\alpha}{1-\alpha^2}b^{(2)}_{3/2}\,. \tag{48}$$

The ratio of Laplace coefficients is given by the continued fraction

$$\frac{b^{(2)}_{3/2}}{b^{(1)}_{3/2}} = \frac{5}{4}\frac{\alpha}{1-}\frac{a\alpha^2}{1-}\frac{b\alpha^2}{1-}\frac{c\alpha^2}{1-}\frac{d\alpha^2}{1-}\cdots \equiv p^{(2)}_{3/2} \tag{49}$$

(Brouwer & Clemence 1961) with $a = -\frac{1}{8}$, $b = \frac{7}{16}$, $c = \frac{1}{16}$, $d = \frac{3}{8}$, etc. Combining and using equation (8) leads to

$$r\frac{dg}{dr} = -g\frac{7 - 2\alpha p^{(2)}_{3/2} + 3\alpha^2}{2(1-\alpha^2)} \equiv -g\Gamma(\alpha)\,. \tag{50}$$

For $\alpha = 0.770$, $p^{(2)}_{3/2} = 0.874$ and $\Gamma = 9.11$.

REFERENCES

Adams, F. C., Ruden, S. P., & Shu, F. H. 1989, ApJ, 347, 959
Applegate, J. H., Douglas, M. R., Gürsel, Y., Sussman, G. J., & Wisdom, J. 1986, AJ, 92, 176
Brouwer, D., & Clemence, G. M. 1961, Methods of Celestial Mechanics (New York: Academic)
Cuzzi, J. N., Lissauer, J. J., & Shu, F. H. 1981, Nature, 292, 703
Duncan, M. J., Levison, H. F., & Budd, S. M. 1995, AJ, 110, 3073
Duncan, M. J., Quinn, T., & Tremaine, S. 1988, ApJ, 328, L69
Fernández, J. A., & Ip, W.-H. 1983, Icarus, 54, 377
———. 1984, Icarus, 58, 109
———. 1996, Planet. Space Sci., 44, 431
Franklin, F., Lecar, M., & Soper, P. 1989, Icarus, 79, 223
Gladman, B., & Duncan, M. 1990, AJ, 100, 1680
Goldreich, P., & Tremaine, S. 1978, Icarus, 34, 240
———. 1980, ApJ, 241, 425
Gradshteyn, I. S., & Ryzhik, I. M. 1965, Tables of Integrals, Series, and Products (New York: Academic)
Grazier, K. R., Newman, W. I., Kaula, W. M., & Hyman, J. M. 1997, preprint
Hahn, J. M., & Ward, W. R. 1998, in preparation
Hahn, J. M., Ward, W. R., & Rettig, T. W. 1995, Icarus, 117, 25 (HWR)
Heppenheimer, T. A. 1980, Icarus, 41, 76
Holman, M. J., & Wisdom, J. 1993, AJ, 105, 1987
Jewitt, D., & Luu, J. 1992, IAU Circ. 5611
Jewitt, D., Luu, J., & Chen, J. 1996, AJ, 112, 1225
Knežević, Z., Milani, A., Farinella, P., Froeschlé, C., & Froeschlé, C. 1991, Icarus, 93, 316
Levison, H. F., & Duncan, M. J. 1993, ApJ, 406, L35
Levison, H. F., Stern, S. A., & Duncan, M. J. 1998, Icarus, in press
Luu, J., Marsden, B. G., Jewitt, D., Trujillo, C. A., Hergenrother, C. W., Chen, J., & Offutt, W. B. 1997, Nature, 387, 573
Malhotra, R. 1995, AJ, 110, 420
———. 1996, AJ, 111, 504
———. 1998, Planet. Space Sci., in press
Morbidelli, A., Thomas, F., & Moons, M. 1995, Icarus, 118, 322
Peale, S. J. 1986, in Satellites, ed. J. A. Burns & M. S. Matthews (Tucson: Univ. Arizona Press), 159
Shu, F. H. 1984, in Planetary Rings, ed. R. Greenberg & A. Brahic (Tucson: Univ. Arizona Press), 513
Soper, P., Franklin, F., & Lecar, M. 1990, Icarus, 87, 265
Stern, S. A. 1995, AJ, 110, 856
———. 1996a, in ASP Conf. Ser. 107, Completing the Inventory of the Solar System, ed. T. W. Rettig & J. M. Hahn (San Francisco: ASP), 209
———. 1996b, AJ, 112, 1203
Stern, S. A., & Colwell, J. E. 1998, Nature, in press
Toomre, A. 1964, ApJ, 139, 1217
Torbett, M. V. 1989, AJ, 98, 1477
Ward, W. R. 1981, Icarus, 47, 234
———. 1988, Icarus, 73, 330
Ward, W. R., & Hahn, J. M. 1998, Science, submitted
Weibel, W. M., Kaula, W. M., & Newman, W. I. 1990, Icarus, 83, 382